Tuning the Exciton Binding Energies in Single Self-Assembled InGaAs/GaAs Quantum Dots by Piezoelectric-Induced Biaxial Stress

F. Ding,[1,2,3,*] R. Singh,[3] J. D. Plumhof,[1] T. Zander,[3] V. Křápek,[1] Y. H. Chen,[2] M. Benyoucef,[1] V. Zwiller,[4] K. Dörr,[5] G. Bester,[3,†] A. Rastelli,[1,‡] and O. G. Schmidt[1]

[1]*Institute for Integrative Nanosciences, IFW Dresden, Helmholtzstrasse 20, D-01069 Dresden, Germany*
[2]*Key Laboratory of Semiconductor Materials Science, Institute of Semiconductors, Chinese Academy of Sciences, Beijing 100083, China*
[3]*Max-Planck-Institut für Festkörperforschung, Heisenbergstrasse 1, D-70569 Stuttgart, Germany*
[4]*Kavli Institute of Nanoscience, Delft University of Technology, P.O. Box 5046, 2600 GA Delft, The Netherlands*
[5]*Institute for Metallic Materials, IFW Dresden, Helmholtzstrasse 20, D-01069 Dresden, Germany*

(Received 3 November 2009; published 12 February 2010)

We study the effect of an external biaxial stress on the light emission of single InGaAs/GaAs(001) quantum dots placed onto piezoelectric actuators. With increasing compression, the emission blueshifts and the binding energies of the positive trion (X^+) and biexciton (XX) relative to the neutral exciton (X) show a monotonic increase. This phenomenon is mainly ascribed to changes in electron and hole localization and it provides a robust method to achieve color coincidence in the emission of X and XX, which is a prerequisite for the possible generation of entangled photon pairs via the recently proposed "time reordering" scheme.

DOI: 10.1103/PhysRevLett.104.067405 PACS numbers: 78.67.Hc, 78.20.hb, 81.05.Ea, 81.40.Tv

Sources of entangled photon pairs *on demand* are a major building block for quantum computation and communication [1]. Recently, the generation of entangled photon pairs from semiconductor quantum dots (QDs) has attracted great interest [2–5]. The polarization-entangled photons are produced in an idealized QD with degenerate intermediate exciton states in the cascade: biexciton (XX) → exciton(X) → ground state (G), where the polarization of a photon pair is determined by the spin of the intermediate exciton state [6]. However, real self-assembled QDs exhibit intermediate exciton ground states split into two states by an energy δ called fine structure splitting (FSS) [7]. This is the consequence of shape and atomistic crystal anisotropy and the electron-hole exchange interactions [8]. The FSS in self-assembled In(Ga)As/GaAs QDs grown along the [001] crystal direction is typically quite large as compared to the radiative linewidth (≈ 1.0 μeV). The nonvanishing FSS encodes the which-path information and destroys the polarization entanglement. The generation of entangled photon pairs by simple preselection of rare dots with δ close to zero [2,4] or by spectral filtering [3] has been demonstrated. Furthermore, a number of postgrowth techniques have been used to reduce δ, such as in-plane magnetic fields [9], lateral electric fields [10,11], uniaxial stress [12], and rapid thermal annealing [13].

An alternative proposal to generate entangled photon pairs from QDs, without any fundamental requirements on the FSS to be smaller than the radiative linewidth, is the so-called time reordering scheme [14]. However, this scheme requires the emission energies of X (E_X) and XX (E_{XX}) to be the same. In this scheme, one entangles the red photons $H1(V2)$ and the blue photons $V1(H2)$ [see the central panel of Fig. 1(a)] across generations in a QD. It is accomplished by performing a unitary operation (time reordering) U on the two-photon state such that $|\langle\phi_H|U_H^\dagger U_V|\phi_V\rangle| > |\langle\phi_H|\phi_V\rangle|$ [14,15], where $|\phi_{H(V)}\rangle$ is the wave packet resulting from the biexciton cascade emis-

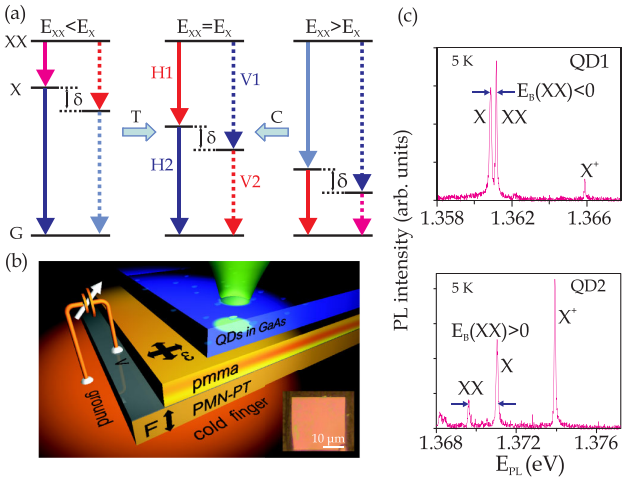

FIG. 1 (color online). (a) Level schemes showing the XX-X cascade. The solid (dashed) line represents the decay channel that yields H (V) polarized photons. Across generation color coincidence of X and XX ($E_X = E_{XX}$) can be achieved by applying tensile (compressive) stress to a QD with positive (negative) $E_B(XX)$. (b) Schematic drawing of the experiment and optical microscopy image of a 200 nm-thick GaAs membrane (inset). (c) Low temperature PL spectra of QDs with negative (QD1) and positive (QD2) XX binding energy.

sion. This novel concept is currently under vivid discussion [15–18]: On one hand the two-photon wave packet may suffer significant dephasing after the time reordering, on the other hand the emission energies E_X and E_{XX} in the as-grown QDs are usually different because of pronounced interactions between charge and spin carriers in a QD.

In this Letter we show that an external biaxial tensile (T) or compressive (C) stress can be used to achieve $E_X \approx E_{XX}$. Stress is provided *in situ* by placing a thin GaAs membrane containing self-assembled InGaAs QDs on top of a piezoelectric actuator, made of $[Pb(Mg_{1/3}Nb_{2/3})O_3]_{0.72}$-$[PbTiO_3]_{0.28}$ (PMN-PT) [see Fig. 1(b)]. With increasing compression, the relative spectral positions of different excitonic species (X, XX, and X^+) show subtle, but systematic changes: The binding energies E_B of both X^+ and XX, defined as $E_B(XX/X^+) = E_X$-E_{XX/X^+} increase in all studied QDs. Based upon million-atom empirical pseudopotential many-body calculations of realistic InGaAs/GaAs QDs, we ascribe this phenomenon to the increase in electron-hole Coulomb interactions due to the increase in confinement of electrons and slight decrease in confinement of holes upon compressive biaxial stress. Finally, different from the behavior observed under in-plane uniaxial stress [12], biaxial strain does not appreciably affect the FSS, a behavior which is also expected from our calculations.

We fabricated 200 nm-thick GaAs membranes with embedded self-assembled InGaAs QDs, and then transferred them onto a 300 μm-thick PMN-PT actuator via PMMA resist [20]. A bias voltage V applied to the PMN-PT results in an out-of-plane electric field F which leads to an in-plane strain $\varepsilon_\parallel$ in the GaAs membrane and the QD structure [see Fig. 1(b)]. The PMN-PT was poled so that $V > 0$ (< 0) corresponds to in-plane compressive (tensile) strain $\varepsilon_\parallel < 0$ (> 0). Figure 1(c) shows low-excitation power photoluminescence (PL) spectra of two QDs with negative $E_B(XX)$ (QD1) and positive $E_B(XX)$ (QD2). The neutral exciton X and the biexciton XX are identified by power- and polarization-dependent PL. (The latter allows us also to determine the FSS of X and XX). An unpolarized line lying at the higher energy side of X and XX is attributed to positive trion X^+ emission. The assignment is supported by the background p-type doping of our structures and by the correlation between $E_B(X^+)$ and $E_B(XX)$ observed in all the studied dots [see Fig. 2(e)].

Figure 2(a) shows the color-coded PL intensity of QD1 as a function of emission energy and voltage V applied to the PMN-PT actuator. V is swept several times between 0 and 1100 V with steps of 20 V, to demonstrate the reversibility of the tuning. For $V > 0$ the QD experiences an in-plane compression (C). The emission energies of different lines show roughly linear blueshifts with V. At the maximum reached bias, E_X shifts by $\sim$1.8 meV, without appreciable deterioration of the emission linewidth and intensity [20]. Similar energy shifts for a given V are observed for different dots in the same device. However,

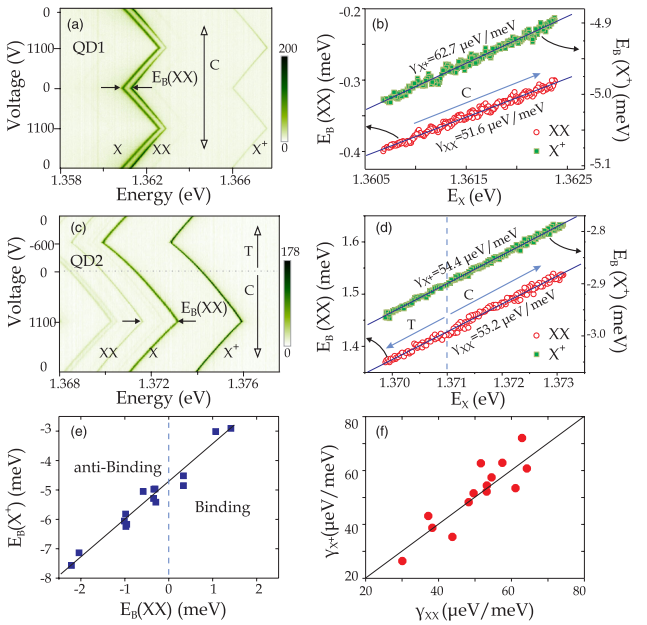

FIG. 2 (color online). Color-coded PL intensity of QD1 (a) and QD2 (c) as a function of emission energy and voltage applied to the actuator. The binding energies of XX and X^+ show a linear increase with E_X for both QDs, as shown in (b) and (d). (e) Binding energies at $V = 0$ and (f) slopes γ_{XX} and γ_{X^+} for 14 different QDs.

different devices show different maximum shifts, which may be due to slight variations in the composition or the mechanical contact of the PMN-PT to the coldfinger. More interestingly, the $E_B(XX)$ and $E_B(X^+)$ show a linear increase with E_X, see Fig. 2(b), with slopes $\gamma_{XX} = 51.6$ and $\gamma_{X^+} = 62.7$ μeV/meV for QD1. The results of a similar experiment performed on QD2 are shown in Figs. 2(c) and 2(d). In this case V is swept to positive and negative values. Under tension ($V < 0$) the QD emission lines redshift and the linear dependence between binding energies and E_X extends also to the tensile (T) strain region.

In order to verify whether these findings are affected by QD structural fluctuations, we have determined the values of γ for 14 different dots. The results are shown in Fig. 2(f). In all the studied dots we observe that both γ_{X^+} and γ_{XX} are *positive* and that for a given dot $\gamma_{X^+} \simeq \gamma_{XX}$. The former observation is interesting as it opens up the possibility to tune $E_B(XX)$ to zero in a controllable way. The latter suggests a common underlying physical mechanism responsible for the changes in binding energy of XX and X^+.

In order to understand the results and estimate the magnitude of the in-plane strain achieved in the experiment, we performed calculations on realistic InGaAs/GaAs QDs containing 3×10^6 atoms using the empirical pseudopotential and the configuration interaction (CI) approaches [21]. The excitonic states are calculated at the correlated CI level, including all configurations generated from 12 electron and 12 hole states (spin included). We model the QD as a lens shaped $In_{0.8}Ga_{0.2}As$ structure with a height of

2.5 nm and elliptical base of major (minor) axis of 10 (7.5) nm along the $[1\bar{1}0]$ ([110]) crystal direction.

Figure 3(a) shows the calculated emission energies of X, XX, and X^+ as a function of biaxial strain $\varepsilon_\parallel = [(a - a_0)/a_0]$, where a (a_0) is the lattice constant of strained (unstrained) GaAs. As in the experiment, all emission lines blueshift for $\varepsilon_\parallel < 0$ and redshift for $\varepsilon_\parallel > 0$. In analogy to the results shown in Figs. 2(b) and 2(d), we plot in Fig. 3(b) the relative binding energies of XX and X^+ as a function of E_X. Although the initial values of E_X and binding energies are somewhat different from those observed in the experiment [Figs. 1(c) and 2(e)], the calculation is able to reproduce the linear increase of $E_B(X^+)$ and $E_B(XX)$ with E_X. For the modeled QD structure the slope of $E_B(XX)$ is $\gamma_{XX} = 114$ μeV/meV, comparable with the experimental values. By repeating similar calculations on a larger QD with a circular base and a height of 3.5 nm with a lower In concentration (60%), we find $\gamma_{XX} = 28.3$ μeV/meV. Although the values of γ's depend on the actual QD structure and size the linear increase of binding energies of XX and X^+ relative to X upon biaxial compression is a rather general phenomenon as we observed in the experiments.

From our empirical pseudopotential calculations, we find that the effect of biaxial strain on the correlation energy is very small. The main changes in the binding energies of XX and X^+ are due to changes in the direct Coulomb interactions between electron and holes and can be approximated by

$$\begin{aligned} \Delta E_B(X^+) &\approx \Delta J_{eh} - \Delta J_{hh}, \\ \Delta E_B(XX) &\approx \Delta E_B(X^+) - [\Delta J_{ee} - \Delta J_{eh}], \end{aligned} \tag{1}$$

where J_{ee}, J_{hh}, and J_{eh} are the Coulomb integrals between lowest electron (e) and hole (h) states. Figure 3(c) shows that ΔJ_{eh} and ΔJ_{ee} increase with compressive strain, with only small deviations from each other. Interestingly, ΔJ_{hh} shows the opposite behavior, but its magnitude is substantially smaller than those of ΔJ_{eh} and ΔJ_{ee}. We thus conclude that the increase in binding energies of XX and X^+ upon compression is mainly a consequence of the increase in the electron-hole attraction term. The fact that $(\Delta J_{ee} - \Delta J_{eh})$ is small, qualitatively explains the similar values of $\Delta E_B(XX)$ and $\Delta E_B(X^+)$, as shown in Fig. 2(f).

To understand the increase in J_{ee}, J_{eh}, and decrease in J_{hh} upon compression, we plot in Fig. 3(d) the strain modified conduction band minimum and the upper two valence bands. For the latter bands we used circles proportional in size to the fraction of heavy-hole character. In the unstrained region, far from the dot, heavy- and light-hole bands are degenerate; close to the dot (inside the dot), the light (heavy)-hole band forms the valence band maximum. Since the QD hole states have up to ~92% heavy-hole character, we define the valence band offset (VBO) as the offset between the heavy-hole bands [Fig. 3(d)]. No such complication arises for the conduction band offset (CBO). In Fig. 3(e) we show a linear increase by ~35 meV for the CBO upon change in biaxial strain from 0.1% to −1%. This represents an increased confinement and localization of wave function: the intuitive picture of a compressed wave function obtained by a compression of the sample, is valid. For the VBO, however, we find a decrease by ~3 meV for the same range of strains. Upon compression, the wave functions tend to become more delocalized. This, rather counterintuitive behavior can be observed directly on the wave functions in Fig. 3(f), where we display the lowest electron state (LUMO) and highest hole state (HOMO) at two different strains. This localization or delocalization gives rise to the increase in J_{ee}, J_{eh}, and decrease in J_{hh} shown in Fig. 3(c). Similar results are obtained also by eight-band kp calculations combined with the CI model [20].

The fact that the biexciton binding energy monotonically increases upon compression provides a controllable strategy to tune $E_B(XX)$ to zero. If XX is initially located at the high (low) energy side of X, a biaxial compression (tension) allows us to tune $E_B(XX)$ so that the color coincidence between XX and X is achievable, depending on the available tuning range, the value of γ_{XX} and the initial value of $E_B(XX)$. Figure 4(a) demonstrates this capability for a QD where $E_B(XX)$ is initially −270 μeV. The total shift of E_X in this device is ~11 meV, which according to the calculations correspond to strain values exceeding ±0.3%. Figure 4(b) shows gray scale coded PL intensity plots of X and XX as a function of linear polarization angle and energy for various values of V. As expected, X and XX

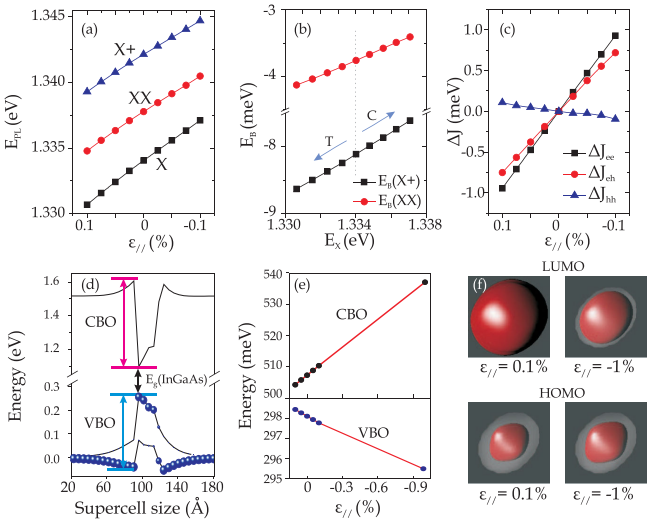

FIG. 3 (color online). (a) Calculated emission energies of X, XX, and X^+ as a function of in-plane biaxial strain $\varepsilon_\parallel$. (b) Relative binding energies of X^+ and XX vs E_X. (c) Changes in Coulomb integrals with biaxial strain. (d) Calculated band offset diagram at $\varepsilon_\parallel = 0$; for the valence band, the size of the circles is proportional to the heavy-hole character of the bands. (e) Changes in CBO (VBO) with strain $\varepsilon_\parallel$. (f) HOMO and LUMO wave functions at $\varepsilon_\parallel = 0.1\%$ and -1%. The red color encloses 75% of the charge density, while light gray color represents the outline of the QD.

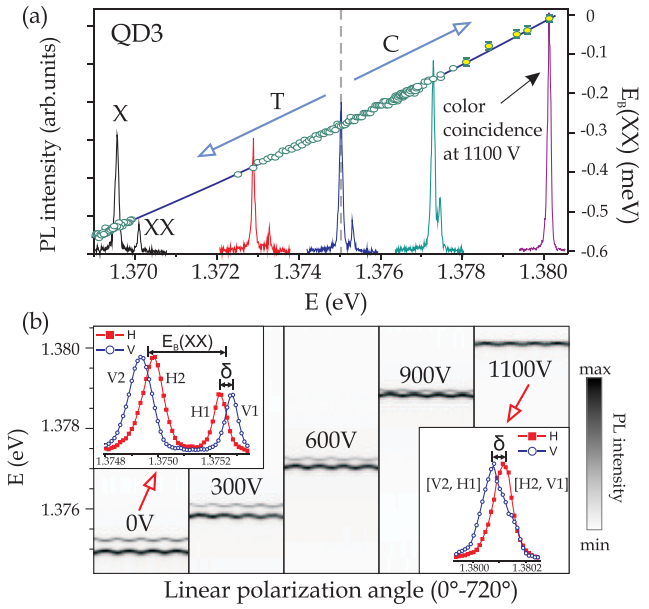

FIG. 4 (color online). (a) Biexciton binding energy of QD3 as a function of E_X. Several spectra are shown, demonstrating the decreasing distance between X and XX with increasing E_X. (b) Polarization-resolved PL map for the X and XX lines at several voltages. At 0 V $E_B(XX)$ is much larger than δ, while $E_B(XX)$ vanishes (limited by the system resolution) and δ dominates at 1100 V.

show anticorrelated shifts as we rotate the analyzer. The FSS for this QD, i.e., the energy separation δ between the H and V components of X or XX is 48 ± 5 μeV. As the voltage increases the magnitude of $E_B(XX)$ decreases, while δ stays constant within the measurement uncertainties. This finding, which is reproduced by our calculations, is not surprising, because the symmetry of the structure is not appreciably changed by biaxial strain. At 1100 V $E_B(XX) \rightarrow 0$ and δ dominates the energy scale in the problem: only two peaks with the splitting of δ can be observed. We have now practically reached the color coincidence of ($V2$, $H1$) and ($H2$, $V1$). For future entanglement measurements, we envision the use of a Michelson interferometer. That will allow the "red" ($V2$, $H1$) and the "blue" ($H2$, $V1$) photons to be directed to the two outputs of the interferometer, and hence spatially separated [22].

In conclusion, we have studied in detail experimentally and theoretically the effect of biaxial strain on the binding energies of different excitonic species confined in single InGaAs/GaAs(001) quantum dots. The most intriguing finding is that biaxial strain is a reliable tool to engineer the QD electronic structure and reach color coincidence between exciton and biexciton emission. While other techniques may be used to reach this goal, such as rapid thermal annealing [13,23] or lateral electric fields [24], strain engineering is advantageous as it can be performed *in situ* and does not produce any appreciable degradation of the emission, which usually occurs at large electric fields [25]. Furthermore, biaxial strain does not alter the excitonic FSS, which should remain sufficiently large for experimental tests on the viability of a newly proposed concept for the generation of entangled photon pairs [14]. Finally, the employed method can be used to study the effect of stress and tune the properties of a broad range of nano- and microstructures, such as optical microcavities [26].

We acknowledge N. Akopian, U. Perinetti, P. Klenovský, C. C. Bof Bufon, R. Hafenbrak, S. Mendach, and P. Michler for fruitful discussions and the financial support of the DFG (FOR730), BMBF (No. 01BM459), NWO (VIDI), CAS-MPG and NSFC China (60625402).

*f.ding@ifw-dresden.de
†g.bester@fkf.mpg.de
‡a.rastelli@ifw-dresden.de

[1] N. Gisin and R. Thew, Nat. Photon. **1**, 165 (2007).
[2] R. J. Young *et al.*, Phys. Rev. Lett. **102**, 030406 (2009).
[3] N. Akopian *et al.*, Phys. Rev. Lett. **96**, 130501 (2006).
[4] R. Hafenbrak *et al.*, New J. Phys. **9**, 315 (2007).
[5] R. Singh and G. Bester, Phys. Rev. Lett. **103**, 063601 (2009).
[6] O. Benson, C. Santori, M. Pelton, and Y. Yamamoto, Phys. Rev. Lett. **84**, 2513 (2000).
[7] D. Gammon *et al.*, Phys. Rev. Lett. **76**, 3005 (1996).
[8] M. Bayer *et al.*, Phys. Rev. B **65**, 195315 (2002).
[9] R. M. Stevenson *et al.*, Phys. Rev. B **73**, 033306 (2006).
[10] B. D. Gerardot *et al.*, Appl. Phys. Lett. **90**, 041101 (2007).
[11] M. M. Vogel *et al.*, Appl. Phys. Lett. **91**, 051904 (2007).
[12] S. Seidl *et al.*, Appl. Phys. Lett. **88**, 203113 (2006).
[13] R. Seguin *et al.*, Appl. Phys. Lett. **89**, 263109 (2006).
[14] J. E. Avron *et al.*, Phys. Rev. Lett. **100**, 120501 (2008).
[15] F. Troiani and C. Tejedor, Phys. Rev. B **78**, 155305 (2008).
[16] G. Pfanner, M. Seliger, and U. Hohenester, Phys. Rev. B **78**, 195410 (2008).
[17] P. K. Pathak and S. Hughes, Phys. Rev. Lett. **103**, 048901 (2009).
[18] J. E. Avron *et al.*, Phys. Rev. Lett. **103**, 048902 (2009).
[19] X. Li *et al.*, Science **301**, 809 (2003).
[20] See supplementary material at http://link.aps.org/supplemental/10.1103/PhysRevLett.104.067405.
[21] G. Bester, J. Phys. Condens. Matter **21**, 023202 (2009).
[22] T. Aichele, G. Reinaudi, and O. Benson, Phys. Rev. B **70**, 235329 (2004).
[23] R. J. Young *et al.*, Phys. Rev. B **72**, 113305 (2005).
[24] M. E. Reimer *et al.*, Phys. Rev. B **78**, 195301 (2008).
[25] M. Korkusinski, M. E. Reimer, R. L. Williams, and P. Hawrylak, Phys. Rev. B **79**, 035309 (2009).
[26] T. Zander *et al.*, Opt. Express **17**, 22 452 (2009).